Morphodynamic changes in the Yangtze Estuary under the impact of the Three Gorges Dam, estuarine engineering interventions and climate-induced sea level rise

Cheng, H. Q.; Chen, W.; Li, J. F.; Jiang, Y. H.; Hu, X.; Zhang, X. L.; Zhou, F. N.; Hu, F. X.; Stive, M. J.F.

DOI
10.1016/j.epsl.2022.117385

Publication date
2022

Document Version
Final published version

Published in
Earth and Planetary Science Letters

Citation (APA)
Cheng, H. Q., Chen, W., Li, J. F., Jiang, Y. H., Hu, X., Zhang, X. L., Zhou, F. N., Hu, F. X., & Stive, M. J. F. (2022). Morphodynamic changes in the Yangtze Estuary under the impact of the Three Gorges Dam, estuarine engineering interventions and climate-induced sea level rise. *Earth and Planetary Science Letters*, *580*, Article 117385. https://doi.org/10.1016/j.epsl.2022.117385

Earth and Planetary Science Letters 580 (2022) 117385

Contents lists available at ScienceDirect

Earth and Planetary Science Letters

www.elsevier.com/locate/epsl

Morphodynamic changes in the Yangtze Estuary under the impact of the Three Gorges Dam, estuarine engineering interventions and climate-induced sea level rise

Cheng H.Q. [a,b,*], Chen W. [c,*], Li J.F. [a,b], Jiang Y.H. [d], Hu X. [e], Zhang X.L. [f], Zhou F.N. [g], Hu F.X. [a], Stive M.J.F. [h]

[a] State Key Laboratory of Estuarine and Coastal Research, East China Normal University, 200062, Shanghai, China
[b] Institute of Eco-Chongming (IEC), 20062, Shanghai, China
[c] Institute of Coastal Systems Analysis and Modeling, Helmholtz-Zentrum Hereon, Max-Planck-Straße 1, 21502 Geesthacht, Germany
[d] Nanjing Center, China Geological Survey, 534 East Zhongshan Road, Nanjing, China
[e] Shanghai Chengtou Group Corporation, 200020 Shanghai, China
[f] Shanghai Municipal Planning and Natural Resources Bureau, 200003, Shanghai, China
[g] Changjiang River Estuary Bureau of Hydrology and Water Resources Survey, Bureau of Hydrology, Changjiang Water Resources Commission, Shanghai, 200136, China
[h] Civil Engineering and Geosciences, Technical University of Delft, PO Box 5048, 2628 CN Delft, the Netherlands

ARTICLE INFO

Article history:
Received 25 March 2018
Received in revised form 17 December 2021
Accepted 14 January 2022
Available online xxxx
Editor: J.P. Avouac

Dataset link: https://figshare.com/s/121deec078d08426cd8a

Keywords:
estuarine turbidity maxima
subaqueous dunes
tidal amplification
sea level rise
Yangtze Estuary

ABSTRACT

The estuarine turbidity maximum (ETM) in the Yangtze Estuary Delta (YED) is muddy by definition and lacks bottom undulations. However, since 2013, a remarkable change has occurred in the YED. Recent images detected by a multibeam echosounder system, SeaBat 7125, for the first time have confirmed widespread regions of subaqueous dunes in the Yangtze ETM channel. This abnormal change is the result of morphodynamic transformation from the combination of an abrupt decline in sediment supply resulting from the construction of the Three Gorges Dam (TGD) and hydrodynamic changes caused by sea level rise. The latter includes anthropogenic-induced sea level rises (from land subsidence and coastal engineering) of 7–37 cm and a climate-induced sea level rise of 8 cm during the past four decades. Obvious evidence of hydrodynamic changes includes tidal amplification, i.e., a 10–28 cm rise in the tidal range, 42–65 cm rise in the lowest tidal level in the dry season, 45–67 cm rise in the highest tidal level in the flood season and 10–30% increase in the amplitude of the major tidal component. These findings will likely have global implications in formulating strategies to combat the superimposed effects of human interventions and climate change on upstream river and downstream coastal developments.

1. Introduction

Many of the world's largest ports and shipping lanes are located in estuaries, and the surrounding land is densely industrially developed and urbanized. High tidal ranges require the construction of expensive coastal defence structures, and high turbidity hampers the access of ships to ports (Schubel, 1968; Grabemann et al., 1997; Mitchell, 2013). On the one hand, enhanced deposition in navigation channels requires intense maintenance dredging (Winterwerp et al., 2013). On the other hand, high suspended sediment concentrations have a negative effect on the ecological functioning of estuarine deltas, as they reduce primary production and cause oxygen deficits (Liu et al., 2018). It is thus of the utmost importance to thoroughly understand the processes that result in tidal and turbidity amplifications (Wang et al., 2019). Only in that way can science-based, effective coastal management strategies be developed to avoid or reduce such problems.

In recent decades, many estuarine systems in Europe (e.g., the Elbe, Ems, and Loire systems) have shown increases in tidal range and turbidity, which seem to be linked to deepening (Winterwerp et al., 2013). The observed changes in estuarine deltas have stimulated many studies focused on their explanations (de Jonge et al., 2014; van Maren et al., 2016). These studies show the importance of tidal amplification and increased flood dominance resulting from deepening and drag reduction by suspended sediment and the presence of sediment sinks.

* Corresponding authors.
E-mail addresses: hqch@sklec.ecnu.edu.cn (H.Q. Cheng), wei.chen@hereon.de (W. Chen).

https://doi.org/10.1016/j.epsl.2022.117385

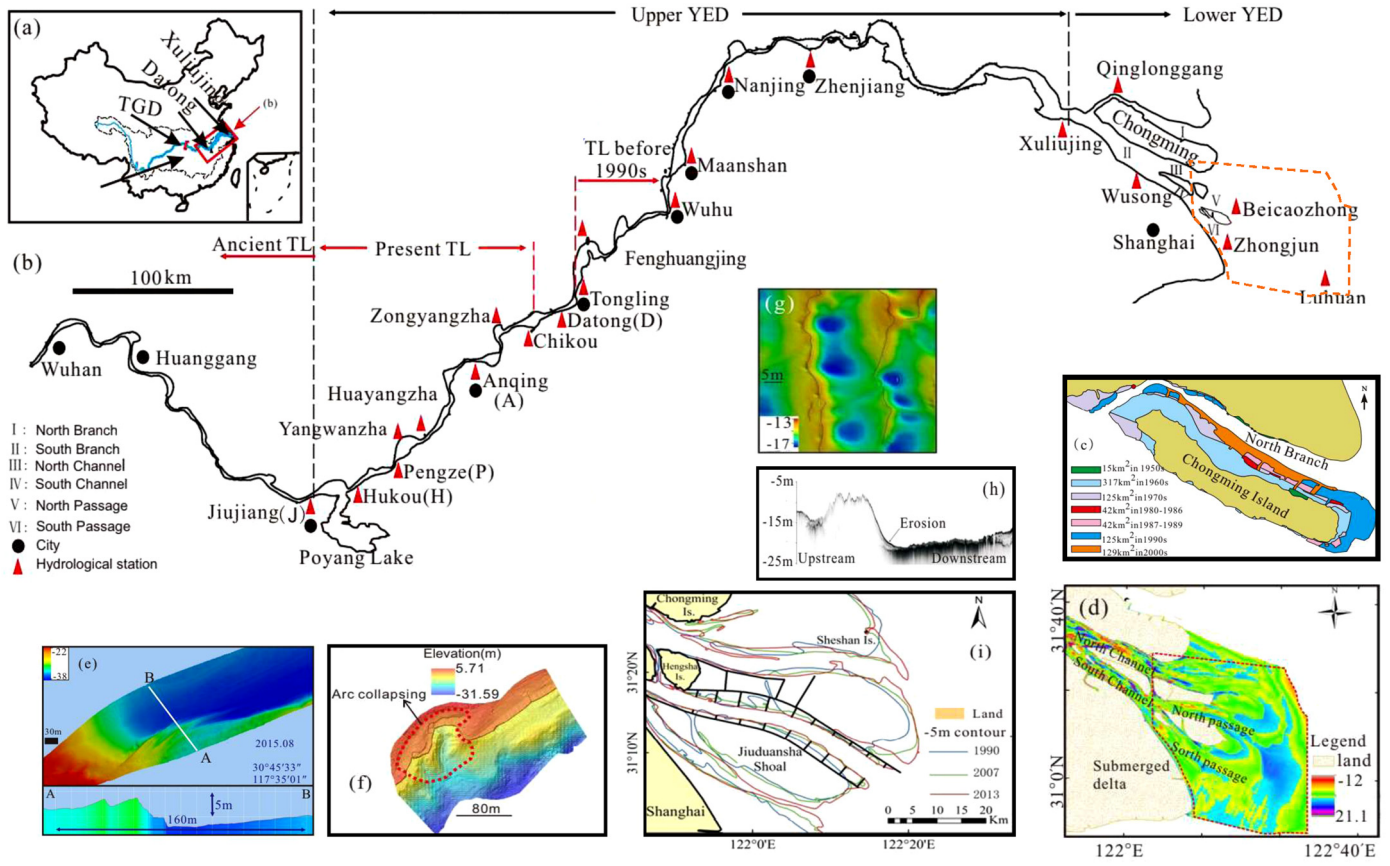

Fig. 1. Study area map and hydrodynamic factor changes in the Yangtze estuarine delta (YED). (a) Study area of the YED. (b) Classification of the YED into the upper and lower YED and classification of the tidal limit (TL) into the ancient TL, present TL and TL before the 1990s in the upper YED. (c) Land reclamation areas in the 1950s, 1960s, 1970s, 1980s, and 1990s–2000s along the North Branch. (d) Changes in the erosion and deposition of three main channels and submerged delta during 1998–2013. (e) Example of a deep scour trough, of which the water depth is 30–50 m and the length is 1320 m, detected by MBES in the lower YED. (f) Example of shore arc collapse detected by a 3D Riegl VZ-4000 terrestrial laser scanner and MBES in the upper YED. (g) Image of catenary-bead subaqueous dunes with erosive holes detected by MBES marked on a distance scale and water depth in the lower left corner in the lower YED. (h) Deep scarp of the channel bed in the North Channel of the lower YED detected by sub-bottom profiler EdgeTech 3100. (i) Changes in the −5 m bathymetry contour in 1990, 2007 and 2013 in the lower YED.

An estuarine delta system that faces problems similar to those of European estuaries is the Yangtze Estuary Delta (YED). Fig. 1 shows the location and geometry of the YED, which is divided into two main reaches. The upper reaches (upper YED) cover the Yangtze River channel from Jiujiang to Xuliujing, and the lower reaches (lower YED) are eastward of Xuliujing until 122.5°E, including submarine dunes above the −5 metre isobath. Analysis of field data collected since the middle of the last century shows significant variations in the morphologies of both estuarine channels and subaqueous deltas, which were naturally generated over a thousand-year period (He et al., 2013; Luan et al., 2016). Notably, the channels within the YED are narrowing due to land reclamation. Among these channels, the North Passage of the YED has been subject to anthropogenic intervention, i.e., it was deepened from 8 metres to 12.5 metres. Furthermore, the construction of dams in the upper reaches of the Yangtze River basin has changed the flow and sediment supply to the YED (Yang et al., 2014). In recent decades, tidal ranges and tidal currents have increased, siltation in navigation channels has intensified, sediment has coarsened (Cheng et al., 2018, 2019), and subaqueous dunes have migrated seaward (Li et al., 2008). Moreover, the North Branch is subject to hyperturbid conditions (with bottom concentrations greater than 10 kg m^{-3}), whereas other branches in the turbidity zone exhibit decreased sediment concentrations at the surface (Jiang et al., 2013a).

These changes lead to the question of whether intensive human interventions in recent decades have altered the natural morphodynamic behaviour that formed over thousands of years and whether this will increase the vulnerability of the YED (Anthony et al., 2014; Tessler et al., 2015). The main objective of the present study is to analyse the natural versus anthropogenically driven behaviour of morphodynamics and hydrodynamics in the YED from the in situ measurements and historical records of subaqueous morphology from the estuarine fronts to the tidal limit and long-term records of the water level, tidal range, amplitude of the major tidal component, and tidal characteristic coefficients at eleven hydrographic stations (Fig. 1).

2. Material and methods

2.1. Subaqueous morphology and bedform data

A series of field campaigns covering different branches within the estuarine turbidity maximum (ETM) region of the YED has been conducted over the past 20 years since 1997 (Table 1, Fig. 2). These measurements show bedform features of this region in typical dry and flood seasons of the Yangtze River. Before 2011, the subaqueous channel bed and slope morphology were measured by using an inner space 24 kHz thermal depth order (TDR) (449 M) and an Ultra 100/325 kHz side scan sonar (SSS) (3050 L) (Cheng et al., 2004). Then, a multibeam echosounder system (MBES) SeaBat 7125 was used for data collection (Li et al., 2008; Wu et al., 2009, 2016a,b; Zheng et al., 2016a,b; Cheng et al., 2019). To obtain data comparable to early measurements, the MBES was operated at 400

Table 1
Details of the subaqueous morphology field campaign in the YED.

Field campaign ceries	Time		Location	Measuring facility
1	Dec. 3^{rd}∼5^{th}, 1997	dry season	South Channel, North and South Passage	TDR SSS
2	Sept. 8^{th}∼9^{th}, 1998	wet season	South Channel, North and South Passage	
3	Dec. 22^{nd}∼23^{rd}, 2000	dry season	South Channel, North and South Passage	
4	May 2^{nd}∼5^{th}, 2002	wet season	South Channel, North and South Passage	
5	Feb. 22^{nd}∼23^{rd}, 2006	dry season	South Channel, North and South Passage	
6	Aug. 20^{th}, 2006	Wet season	South Channel, North and South Passage	
7	Mar. 20^{th}∼30^{th}, Sept. 20^{th}∼30^{th}, 2008	wet season	North and South Channel, Passage	
8	Jan. 26^{th}∼Feb. 2^{nd}, 2010	dry season	North and South Channel, Passage	
9	Dec. 8^{th}∼12^{th}, 2011	dry season	North and South Channel, Passage	
	Jun. 6^{th}∼10^{th}, 2012	wet season	North and South Channel, Passage	
10	Jun. 19^{th}–20^{th}, 2013	wet season	North and South Channel, Passage	MBES
11	Jun. 28^{th}–30^{th}, 2014	wet season	North and South Channel, Passage	
12	Jun. 23^{rd}, Jul. 27^{th}–Aug. 15^{th}, 2015	wet season	North and South Channel, Passage	
13	Aug. 31^{st}∼Sep., 28^{th}, 2016	wet season	North and South Channel, Passage	

Inner Space 24 kHz Thermal Depth Recorder (449M) (TDR).
Ultra 100/325 kHz Side Scan Sonar (3050L) (SSS).
Reson SeaBat 7125 Multi-beam Eco-sounding System (MBES).
Geo-Chirp.

kHz, and the transducer was fixed to the left side of the surveying ship by cables and a custom-made shelf. The boat velocity was maintained at approximately 2.5 m/s, and the ping was 20 Hz. The final multibeam data were processed by using draft correction and sound speed correction. Moreover, roll, pitch, and yaw calibrations were conducted. Abnormal beam signals were removed in the editing module by using PDS 2000 software. The positions were fixed by using a Trimble-R8 real-time differential global positioning system (DGPS).

2.2. Aquatic channel slope morphology data

Using a Riegl VZ-4000 Terrestrial Laser Scanner (TLS), field measurements were collected at four sites, i.e., Nanjing, Tongling, Maanshan, and Hukou, along the main channel of the upper YED (see Fig. 1b). The instrument was set in a wide field of view ($60°\times360°$), the laser pulse repetition rate (PRR) (peak) was set to 50 kHz, and the vertical and horizontal resolutions were 0.013 and 0.03, respectively. The positions and elevations of four reflection targets at four flow stations were fixed by using an R7GNSS+R 8GNSS system with GPS points and were calibrated to the project coordinate system (PRCS) of the TLS.

2.3. Land reclamation area data

Considering the intensive artificial narrowing of the North Branch in a short period (approximately the 1950s), we analysed land reclamation in the North Branch as an example to illustrate the anthropogenic impact on estuarine morphologic evolution. Topographic maps of the North Branch were made by Admiralty charts (1:25,000 scales) from the Maritime Safety Administration of the People's Republic of China and local Admiralty charts (1:2,000; 10,000). Available historical maps since the 1950s, when intensive land reclamation started, were collected and digitized (Fig. 1c).

2.4. Historical bathymetric data

Two sets of navigational charts were collected. The first set is the navigational charts of the upper YED from Jiujiang to Xuliujing in 1998 and 2013. The second set is the navigation charts in the lower YED between 1879 and 2015 (Fig. 1b). Note that different tidal datums were used in these charts, such as an extreme low tidal datum in 1879, the lowest low tidal datum in 1953, the theoretical depth datum during 1959 and 1988 and the theoretical lowest tidal datum during 1990 and 2015. These tidal datums were united by using the Mercator projection and the 1954 Beijing coordinate system. Digitization of charts was completed in ArcGIS 10.2, and digital elevation models (DEMs) were constructed through the kriging method. Subsequently, deposition and erosion in the study area were calculated by comparing DEMs in different years.

2.5. Grain size of bed sediments

Sixty bed sediment samples were collected along the main channel of the YED. The particle size distribution of bed samples was analysed by using a Mastersizer 2000 laser granulometer in the laboratory. Organic matter and $CaCO_3$ concentrations were removed by using 10% H_2O_2 and 10% HCl. An appropriate amount of Na_2PO_3 was used for each of 60 samples.

2.6. Tidal level data and analysis methods

Three sets of tidal level data for the estimations of extreme tidal level, tidal range, and tidal constituents were collected in this study. The first set is the hourly measured tidal level data at 9 tidal gauge stations, namely, Chongxi, Nanmen, Baozhen, Wusong, Sanjiagang, Zhongjun, Niupijiao, Luhua, and Luchaogang, in the lower YED between 1974 and 2013 (Fig. 1b). This data set was used to calculate decadal sea level rise (SLR) by using the lowest normal low tidal level with thirteen shallow water tidal harmonic constituents (M2, S2, K1, O1, M4, and MS4) (Raymond et al., 2004). The second set is the hourly measured tidal level data at Qinglonggang tide gauge station between 1989 and 2000 (Fig. 1b). This data set was used to verify the relative SLR contributed by land reclamation along the North Branch. The third set is the hourly measured water level data between 2007 and 2016 at 12 hydrographic gauge stations along the main channel of the upper YED: Jiujiang, Hukou, Yangwanzha, Huayangzha, Anqing, Zongyangzha, Chikou, Datong, Tongling, Fenghuanjing, Wuhu and Nanjing (Fig. 1b).

2.7. Spectral analysis

To determine the tidal limit (TL) in the upper YED, water level measurements at 12 stations (see section 2.6) between 2007 to

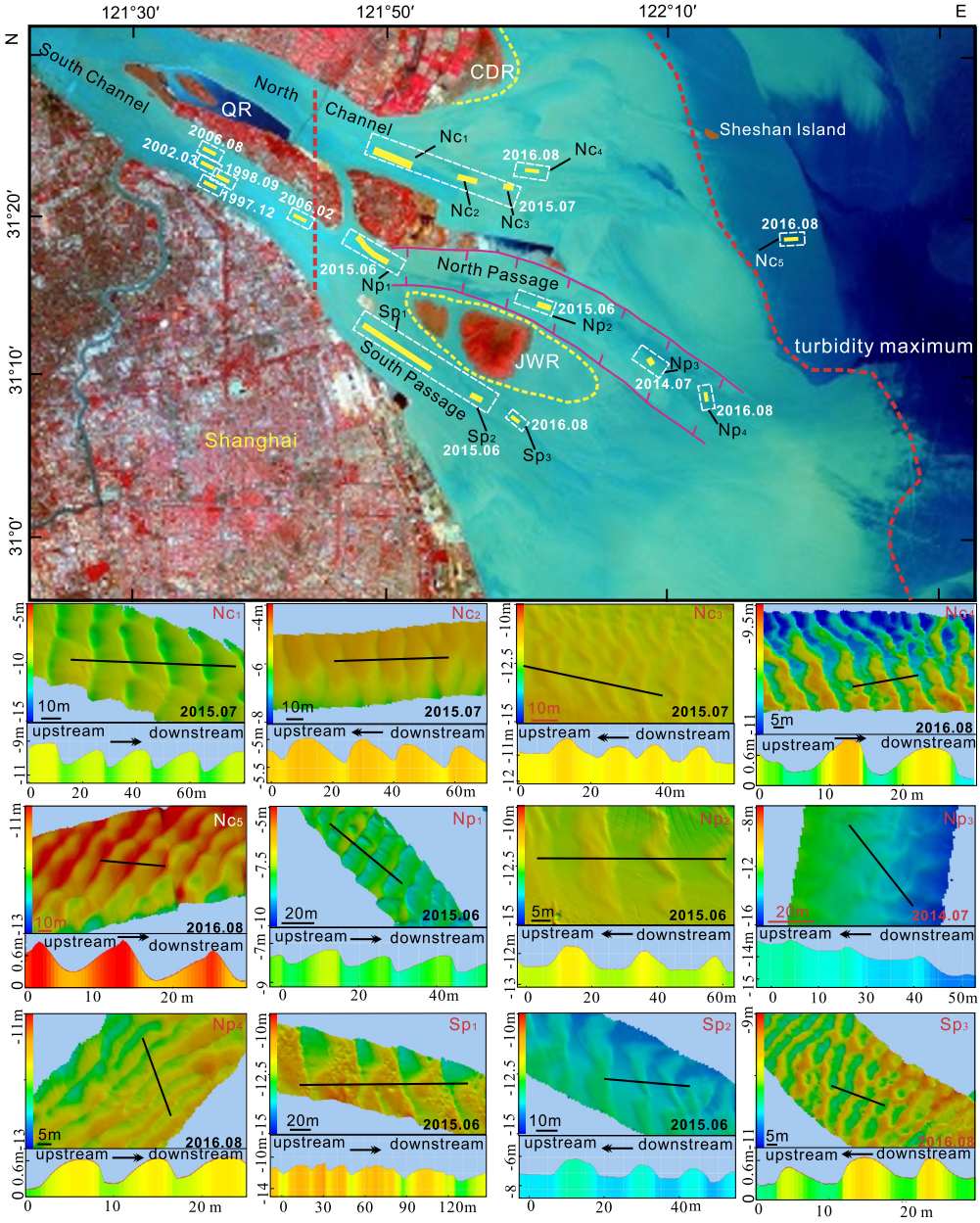

Fig. 2. Measured subaqueous dunes in the main channels on the satellite image showing the estuarine turbidity maximum (ETM) of the YED between two red dashed lines in light green. Upper panel: the white dashed rectangles denote sections where the subaqueous dunes occur in the main channels: South Channel, North Channel (NC), North Passage (NP) and South Passage (SP). The northern and southern dikes of the Deep Waterway are shown as red solid lines along the North Passage. The measured transects are shown as yellow solid lines. Lower panel: enlarged view of subaqueous dunes in each of the measured channels and transects: Ncl, Nc2, Nc3, Nc4, Nc5, Npl, Np2, Np3, Np4, Spl, Sp2, and Sp3. They were detected by a Teledyne Reson Seabat 7125 multibeam echosounding system in 2014, 2015, and 2016. The abbreviations CDR and JWR, with the yellow dashed line, represent the Chongming Dongtan Reserve and Jiuduansha Wetland Reserve, respectively. Ncl, Nc4, Npl and Spl on the lee side are oriented seaward, while Nc2, Nc3, Np2, Np3 and Sp2 on the lee side are oriented landward.

2016 were analysed with a spectral analysis method. All the data were sorted into one-hour intervals and outliers were excluded. In order to reduce the impact of non-tidal fluctuations, such as ship transportation, sluice dispatch, and the effect of seasonal climate change on water level changes, 80 short-term data sets of 5–10 days, showing relatively smooth water level changes, were selected from the data for spectrum analysis. Each individual data set is transformed into a Fourier function by using:

$$\eta = (x - \mu)/\sigma \tag{1}$$

in which η is the standardized water level, x is the measured water level, μ is the sample average, σ is the standard deviation. Eq. (1) is tested with red noise of the first order auto regressive model (Braun et al., 2009) to assess the significance of the TL.

3. Results

3.1. Channel erosion

In the upper YED, a significant riverbed erosion together with bedload coarsening appeared in more than 75% of the main channel during 1998-2013 (Fig. 1b). This is directly related to the Three Gorges Dam project. The construction of the Three Gorges Dam caused a blockage of a large amount of sediment from the upper reaches of the Yangtze River in the reservoir area. From 2003 to

2013, this amount reached 15.3×10^8 m^3. Due to the reduction in the sediment supply, the amount of erosion in the upper YED area during the same period reached 4.2×10^8 m^3, which is equivalent to 26% of the total amount of sediment that should have entered the upper YED but is now trapped upstream of the dam. In the lower YED, strong erosion was observed in the four main bifurcated channels, i.e., North Channel, North Passage, South Channel and South Passage, during a similar period 1998–2013 (Fig. 1d). Preliminary studies have qualitatively shown connections between the trapping of sediment in the TGD reservoir and the erosion in the YED (Zhang et al., 2018; Zheng et al., 2018) and demonstrated the response of the submarine delta (e.g., Jiuduansha shoal) evolution to the variation in sediment supply from the Yangtze watershed. However, quantitative connections between the erosion of the estuary channel and the incoming sediment in the drainage basin are still unclear.

Five novel types of subaqueous erosive bed morphologies were observed in the YED. Typical examples are shown in Fig. 1: deep scour troughs (Fig. 1e), collapsing shore arcs (Fig. 1f), catenary-bead subaqueous dunes (Fig. 1g), deep scarps (Fig. 1h) and strong local scouring (Fig. 1i). Catenary-bead subaqueous dunes with holes have been widely scattered in both the upper and lower YED since 2014 (Zheng et al., 2016a). A widely scattered deep scour trough with a depth of 10–30 m and length of 30–5000 m and shore arcs collapsing along the main channel of the upper YED were observed in our field campaigns during both 2015 and 2016 (Zheng et al., 2016b). Deep scarps and strong local scouring have occurred since 2013 around the basement of Sheshan Island, the North Channel, and the eastern head of the north jetty of the Deep Waterway in the North Passage (Fig. 1i), where an intensive siltation area developed. The widespread appearance of new types of subaqueous erosive bed morphologies reveals that the sediment received in the subaqueous deltas in recent years is insufficient to support the hypothesis of a fast progradation of the YED.

3.2. Sandy subaqueous dunes in the muddy ETM

Sandy dunes appear on the channel bed of the South Branch and middle South Channel from 1997 to 2002 and moved seaward approximately 11.7 km to the low South Channel from 2002 to 2006 (Li et al., 2008), while they did not occur in the North Channel. The sandy dunes kept moving downstream from 2006 to 2012, and were still outside of the ETM (Fig. 2). In the dry season and flood season, the mean dimensions of the dunes were 14.1 m and 41.4 m in wavelength and 0.6 m and 1.6 m in height, with length-height ratios of 23.5 and 25.9, respectively. The year 2013 was likely a turning point of the subaqueous morphologic evolution in the ETM of the YED. Our most recent multibeam echosounder records (campaigns 11∼13, Table 1) demonstrate a region of widely scattered subaqueous dunes in the ETM (Fig. 2). In the North Channel (NC), North Passage (NP) and South Passage (SP), the mean dimensions of dunes were 18.0 m, 23.5 m, and 21.3 m in wavelength and 0.9 m, 0.5 m, and 0.8 m in height, with length-height ratios of 19.3, 45.1, and 26.6, respectively. The landward boundary of dunes in the three channels moved seawards for 20.9 km, 6.6 km, and 29 km, respectively. In general, the migration of these dunes shows two orientations, i.e., seaward (Fig. 2; Nc1, Nc4, Nc5, Np1, Sp1, and Np4) and landward (Fig. 2; Nc2, Nc3, Np2, Np3, and Sp3). Note that Nc5 is located outside the ETM.

These dunes are completely different from the channel morphology observed before 2013 or that previously documented (Li et al., 2008; Cheng et al., 2018). Early field studies (e.g., campaigns 1∼6, Table 1) also revealed similar sandy subaqueous dunes, but only outside the ETM (see Fig. 2 for the locations). To our knowledge, this is the first time that subaqueous dunes have been observed in the YED. It is also the first report in the world on the appearance of subaqueous dunes on a short time scale in the ETM, which is an area that is usually known for muddy deposition and transport.

3.3. Amplification of hydrodynamics in the estuary

The tidal range is one of the significant contributors to coastal inundation. Therefore, it is very important to investigate the dynamics of tidal range variations on different time scales. Regarding the seasonal mean sea level at the stations, the results show that the coastal sea level can be increased by baroclinity itself, since river runoff freshens coastal water in the baroclinic mode, and thus, the local sea level increases due to steric effects. Consequently, the increased sea level could further weaken the damping effect. However, this has a relatively minor impact on the tidal range.

Until the 1990s, the upper limit where the impact of tides on water elevation could reach was around Datong station (see Fig. 1), which is approximately 630 km upstream from the estuary mouth. This was often observed during the spring tide in the dry season of the Yangtze River, when the runoff was weak and the tide was strong (Shi et al., 2018). However, the spectral analysis of the recent water level data collected at 12 hydrographic stations from Jiujiang to Wuhu between 2007 and 2016 reveals that the TL migrated upstream to Jiujiang. As shown in Figs. 3a and b, a power spectral density (black line) higher than the noise (red curve) value indicates the existence of a semidiurnal tidal signal (dashed black line) in each individual water level data set. The TL moves back and forth in the reach between Jiujiang and Anqing ca. 220 km in response to the seasonal variations in water discharge (Fig. 3c). Moreover, consistent mean water level rises of 22 cm, 24 cm, and 23 cm were detected at different hydrographic stations along the upper YED reach between 2008 and 2015 (Fig. 3f). The upstream limit, Jiujiang, was reached in the dry season of 2007 when an extraordinary dry event occurred (Shi et al., 2018). This location was ca. 850 km from the East China Sea. The last time that a TL was observed at Jiujiang, the event was documented by archaeological literature from the Jin Dynasty, which is more than 2 ka ago. It is worth emphasizing that during that time, the Yangtze River mouth was located around Zhenjiang (see Fig. 1b for the location), which is 300 km upstream from the present-day estuary mouth (Shi et al., 2018). In other words, the length of the upper YED remained for two thousand years until the 1990s but extended by 30%, with the TL moving upstream ca. 220 km, in the past three decades.

Moreover, in the lower YED, amplified hydrodynamics are illustrated by a significant increase in the highest high tidal level and the lowest low tidal level, tidal constituents of M_2, S_2, and M_4 and an obvious decrease in K_1 O_1, and MS_4 (Table 2). The local tidal datum rose from 15 cm to 43 cm over the last four decades (Fig. 3d). The regional mean sea level rose at the three tidal gauge stations of Wusong, Zhongjun and Luhua (Fig. 1b, Fig. 3e). The mean high tidal level rose 27 cm from 1989 to 1998 at Qinglonggang tidal gauge station (Fig. 3g). There is an obvious relationship between hydrodynamic amplification and local coastal engineering works. Fig. 3h illustrates the consistency between the rise in annual mean tidal levels larger than 4 m at the Qinglonggang tidal gauge station and land reclamation along both sides of the North Branch.

4. Discussion

Estuaries are impacted simultaneously by runoff from the river side and tidal forcings from the marine side. Through the interactions between geometry and hydrodynamics, an estuary often illustrates a topography that adapts to a certain morphodynamic equilibrium. Savenijie (2012) investigated alluvial estuary shapes

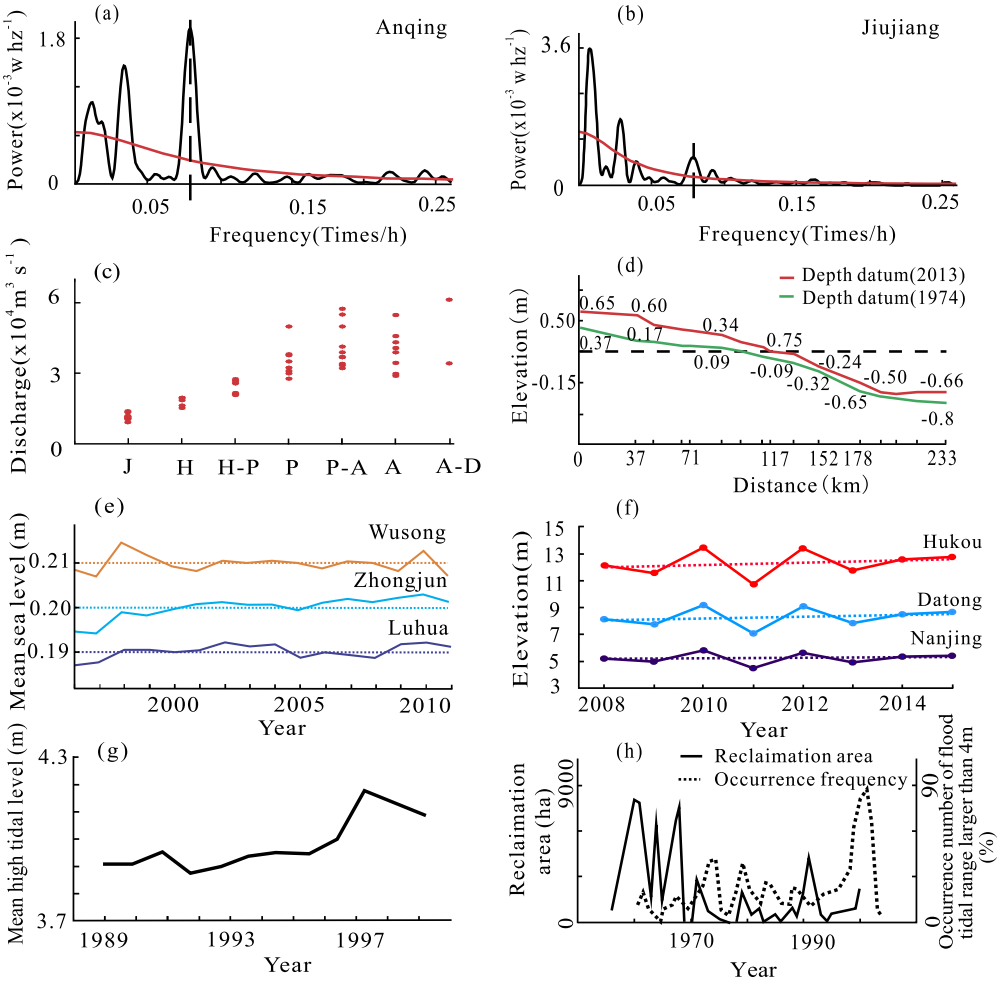

Fig. 3. Variation in the annual mean water level above the local Wusong elevation datum in the YED. (a) Spectral analysis of the water level at Anqing station in response to a discharge of 38500 m^3/s at Jiujiang station. (b) Spectral analysis of the water level at Jiujiang station in response to a discharge of 9800 m^3/s at Jiujiang station. Here, the black line represents the power spectral density curve, and the red line represents the red noise curve. (c) Relationship between the location of TL at Jiujiang (J), Hukou (H), the reach between Hukou and Pengze (H-P), Pengze (P), the reach between Pengze and Anqing (P-A), Anqing (A) and the reach between Anqing and Datong (A-D) and the synchronous discharge at Jiujiang station, a reference station for water discharge. (d) Difference in the theoretical tidal datum from Xuliujing (0 km) to Luhua (233 km) between 1974 and 2013. (e) Variation in the annual mean sea level (MSL) between 1996 and 2011 at the Wusong, Zhongjun and Luhua tidal gauge stations in the lower YED (LYED). (f) Variation in the annual mean water level at Hukou, Datong, and Nanjing in the upper YED (UYED). (g) Variation in the annual mean high tidal level at the Qinglonggang tidal gauge station. (h) Relationship between the area of land reclamation and the frequency of the occurrence of high tidal levels larger than 4 m at the Qinglonggang tidal station.

Table 2
Recent four decadal changes of tidal constituents (TC) in the lower Yangtze Estuary.

TC	Nanmen		Baozhen		Wusong		Zhongjun		Luchaogang	
	C (cm)	A (%)	C (cm)	A (%)	C (cm)	A (%)	C (cm)	A (%)	C (cm)	A (%)
M_2	8.36	9	5.38	5	0.54	1	3.94	3	17.14	12
S_2	10.81	32	8.68	24	1.84	4	2.89	6	6.97	13
K_1	−0.38	−2	0.00	0	0.08	0	−0.22	−1	−0.75	−2
O_1	−1.40	−8	−1.76	−11	0.94	6	0.41	3	2.03	12
M_4	1.07	6	−0.62	−4	−0.24	−1	−1.85	−13	−0.31	−3
MS_4	−4.80	−23	−6.01	−32	0.84	6	−1.39	−12	0.63	8

TC: Tidal constituent; C: Change; A: Amplitude.

on a global scale with external tidal forcing, which are characterized by the observed rate of tidal damping:

$$\delta_H = \frac{1}{H}\frac{\partial H}{\partial x} \tag{2}$$

Here, H is the tidal range and x is the along-estuary location. This classifies estuaries into three types, i.e., ideal, amplified and damped estuaries. In the first case, $\delta_H = 0\ m^{-1}$ suggests an estuary, where along the channel upstream, tidal energy that is lost due to friction (by freshwater in the river and the estuary bottom) exactly compensates for the energy gained through channel convergence. In the second type, $\delta_H > 0\ m^{-1}$, the frictional effect is smaller than that of the channel convergence, and the tidal range is amplified upstream. In the third type, $\delta_H < 0\ m^{-1}$, friction is strong where channel convergence is weak, and the tidal range is damped along the estuary. It is worth noting that in one estuary, the tidal range can be damped faster (with a more negative δ_H), while the tidal range itself is amplified. Using spring tide tidal range data, we computed the damping rate in the lower YED for

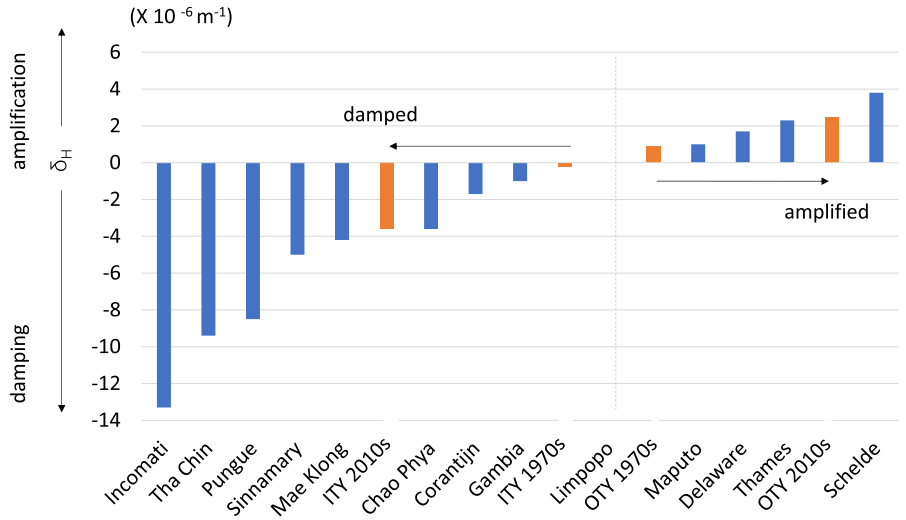

Fig. 4. Recent decadal amplification of hydrodynamics in the Yangtze Estuary compared with different types of estuaries around the world.

the 1970s and 2010s. The results are shown in Fig. 4 and compared with different types of estuaries around the world, where tidal damping rates are available in Savenijie (2012). Note here that we examine δ_H inside the turbidity maxima of the Yangtze Estuary (ITY) and outside the turbidity maxima of the Yangtze Estuary (OTY) separately, regarding distinct hydrodynamic conditions. The lower YED was close to an ideal estuary in the 1970s. However, in the 2010s, the estuary developed in the opposite direction such that the tide became more damped inside of the turbidity maxima, while it was amplified in the upstream branch outside of the turbidity maxima.

The changes in the tidal range damping rate reflect the relative intensity of friction over channel convergence before and after recent human intervention and climate change. Considering the slight impact of the Three Gorges Dam on the water levels of the YED (Zheng et al., 2021), the local sea level rise in the YED is estimated from our historical data analysis at Wusong tidal gauge station. Our recent analysis distinguished the local sea level rise from anthropogenic-induced sea level rise (including land subsidence and coastal engineering) of 7–35 cm and the climate-induced sea level rise of 8 cm (Cheng and Chen, 2017; Cheng et al., 2018). These results are different from the eustatic SLR projections of ca. 2 mm a^{-1} scenarios with climate warming by 2030 (Jevrejeva et al., 2016; Dieng et al., 2017; IPCC R6, 2021) and appear to be the main reason for the reduced friction in the YED. The latter causes the amplification of the tidal range in the OTY as well as the upper YED and thus the upstream migration of the tidal limit. Inside the ETM, SLR also causes a reduction in bottom friction. However, the massive channel narrowing and construction of the regulational dike-groyne system in the 2000s has considerably increased friction from the side banks (Pan et al., 2012; Jiang et al., 2012, 2013b; Wang et al., 2022). Moreover, land reclamation on shallow shoals, e.g., the East Hengsha Shoal (Jiang et al., 2013a; Du et al., 2016; Wu et al., 2016a,b; Mei et al., 2018) and the East Nanhui Shoal (Zhang et al., 2018; Wei et al., 2017), reduces channel convergence. Land reclamation, which has led to the narrowing and fixing of the channel, caused the length of the turbidity maximum zone to decrease: its landward boundary shifted 5 km seaward during spring tide and 17 km seaward during neap tide in the dry season from 2006 to 2019 (Teng et al., 2021). At the end, inside the ETM, where friction greatly outweighs channel convergence, tidal damping is enhanced.

In addition to the influence of these coastal engineering projects in the YED, the impact of human interventions from watershed dam construction is mainly on the sediment supply, both suspended and bed load, which has declined by 60% in recent years (Yang et al., 2018). This explains the more frequent occurrence of channel erosion in the upper YED. In the ETM, such a reduction in sediment load is superimposed on the effect of the increase in friction and causes intensive erosion in various channels. Note that this situation does not apply to the North Branch. This is because early land reclamation (in the 1960s–1970s) occurred mainly in the upper part of the channel, which has greatly eliminated the width of the riverside entrance and increased channel convergence (Fig. 1c). The North Branch has turned into a tidally dominant estuary, of which the main source of the sediment load is from the marine side rather than from the Yangtze side (Zhang et al., 2015; Guo et al., 2021).

Dalrymple et al. (1992), based on the relative influence of tidal, river and wave processes, studied the morphology of alluvial estuaries and classified estuaries worldwide into different types. In this framework, the YED is projected onto the plane as a type of prograding delta (see Fig. 3 of Dalrymale et al., 1992) according to data sourced from published literature (Chen et al., 1985). A similar estuary of this type is the Mississippi Delta. As a consequence of channel narrowing and land reclamation on shallow shoals, the area of the YED entrance decreases, causing a decrease in the tidal prism in the ETM. Using a numerical model, Zhang et al. (2018) computed tidal prisms around the North Passage seaside entrance, which in 2010 was approximately 2×10^9 m^3 less than that before the construction of the Deep Waterway Project. However, this does not imply that the lower YED would develop in the direction of the Mississippi Delta, although the fluvial sediment source is considerably reduced. On the other hand, although the channels of the ETM experience severe erosion, the reduced water and sediment exchange between shoals and channels could potentially enhance the trapping of sediment on the shallow shoals and tidal bars. Zhang et al. (2018) illustrated positive feedback between the decreased tidal prism and eliminated offshore sediment flushing, which offsets the negative impact of sediment supply reduction on shoal accretion.

Clearly, recent changes in hydrodynamic and sediment transport due to the combined influence of local and nonlocal intensive human interventions, together with SLR, from climate change have triggered new erosional and depositional patterns in the YED, i.e., the channels have become deeper, and shoals have grown higher rather than larger. Whether these morphodynamic configurations at the decadal timescale could destabilize the YED channel-shoal system and lead to a new morphological configuration in the long term is still unclear and deserves more systematic studies in the

near future. This research is also relevant for developing effective and sustainable adaptation strategies for flood protection and fresh water supply in estuarine delta cities in response to new SLR projections in ca. 2 m scenarios with climate warming above 1.5 °C–2 °C by 2100 and other potential human interventions in the coming decades.

5. Conclusions

Through the collection of historical bathymetry, water level, current, and sediment data in the YED from the 1950s and a series of field measurements of subaqueous morphology covering 20 years since 1997, we systematically analysed the change in erosional and depositional patterns in the YED under the TGD and coastal engineering impact with climate-induced sea level rise. Many bed erosion events with new shapes have been found in our multiyear field campaigns since 2013, and the YED is developing in a new pattern regarding deltaic morphodynamics. The YED can be divided into two zones, i.e., outside and inside turbidity maxima, with regard to the changes in tidal dynamics. Outside the turbidity maxima, the tidal influence is amplified, leading to the upstream migration of the tidal limit. Inside the turbidity maxima, although the tidal range is amplified in the channels under human intervention, it is damped faster upstream with a narrowing channel width and reducing convergence. Together with the drastic reduction in sediment supply by the construction of the TGD, most of the channels in the YED have experienced erosion, especially inside the turbidity maxima. Widely scattered subaqueous dunes are observed in the North Passage and South Passage, which is the first time that the appearance of sandy subaqueous dunes in a muddy ETM has been reported worldwide. Such channel erosion combined with the accretion of shallow shoals prevents the shoals from growing larger rather than higher, which seems to be a morphodynamic configuration of the YED in the near future.

CRediT authorship contribution statement

Cheng, H.Q. conceived the study and has conducted long-term field measurements since the 1990s. **Chen, W.** contributed to the ideas in the discussion and was responsible for ensuring the accuracy of the descriptions and proofreading. **Li, J.F.** conceived the partial survey of subaqueous dunes. **Jiang, Y.H.** conceived a partial survey and collected data on the water level of the upper YED. **Hu, X.** conceived the partial survey of channel erosion. **Zhang, X.L.** conceived the urban land subsidence data and historical bathymetric channel data in the YED. **Zhou, F.N.** conceived the tidal level data collection and analysis in the YED. **Hu, F.X.** contributed the idea of TL change. **Stive, M.J.F.** contributed to the quality control of research and language.

Declaration of competing interest

The authors declare that they have no known competing financial interests or personal relationships that could have appeared to influence the work reported in this paper.

Data availability

All data sets used in this study are publicly available at https://figshare.com/s/121deec078d08426cd8a.

Acknowledgements

We thank the NSFC-NWO-EPSRC for financial support through the joint project of natural versus anthropogenically driven behaviour of hydrodynamics and sediment dynamics in estuarine delta systems with application to the Yangtze Estuarine Delta (51761135023); the NSFC through the projects of the response mechanism of sediment entrapment and subaqueous dunes in the large engineering projects in the Changjiang estuary (41476075, 51479074, 41340044, 40776056, 40576048, 49571007, and 51061130544); the China Geological Survey through the comprehensive survey of the geological environment along a major engineering area of the Changjiang River (DD20160246); and the Shanghai Science and Technology Committee through the impact and key adaptative technology of sea level rise on the security of Shanghai municipality project (10dz1210600). The author Heqin Cheng also greatly thanks Prof. Huib E. de Swart from the Institute for Marine and Atmospheric Research Utrecht, Utrecht University of the Netherlands for suggestions that improved the quality of the manuscript.

References

Anthony, E.J., Marriner, N., Morhange, C., 2014. Human influence and the changing geomorphology of Mediterranean deltas and coasts over the last 6000 years: from progradation to destruction phase? Earth-Sci. Rev. 139 (5), 336–361.
Braun, H., Ditlevsen, P., Kurths, J., Mudelsee, M., 2009. Limitations of red noise in analysing Dansgaard-Oeschger events. Clim. Past Discuss. 6 (1), 85–92.
Chen, J., Zhu, H., Dong, Y., Sun, J.M., 1985. Development of the Changjiang estuary and its submerged delta. Cont. Shelf Res. 4 (1), 47–56.
Cheng, H.Q., Kostaschuk, R., Shi, Z., 2004. Tidal currents, bed sediments, and bedforms at the South branch and the South channel of the Changjiang (Yangtze) estuary, China: implications for the ripple-dune transition. Estuaries 27 (5), 861–866.
Cheng, H.Q., Chen, J.Y., 2017. Adapting cities to sea level rise: a perspective from Chinese deltas. Adv. Clim. Change Res. 8, 130–136.
Cheng, H.Q., Chen, J.Y., Chen, Z.J., Ruan, R.L., Xu, G.Q., Zeng, G., Zhu, J.R., Dai, Z.J., Chen, X.Y., Gu, S.H., 2018. Mapping sea level rise behavior in an estuarine delta system: a case study along the Shanghai coast. Engineering 4 (1), 156–163.
Cheng, H.Q., Teng, L., Chen, W., 2019. Dune dynamics in coarse silt, sand and gravel along the main channel from the estuarine front of Yangtze River to the Three Gorges Dam. In: Proceedings of International Conference Maine and River Dune Dynamics (MARID VI). 1-3 April 2019, Bremen, Germany. ISBN 978-2-11-139488-9, pp. 45–50.
Dalrymple, R.W., Zaitlin, B.A., Boyd, R., 1992. Estuarine facies models: conceptual basis and stratigraphic implications. J. Sediment. Petrol. 62 (6), 1130–1146.
de Jonge, V.N., Schuttelaars, H.M., Beusekom, J.E.E.V., Talke, S.A., de Swart, H.E., 2014. The influence of channel deepening on estuarine turbidity levels and dynamics, as exemplified by the Ems estuary. Estuar. Coast. Shelf Sci. 139, 46–59.
Dieng, H.B., Cazenave, A., Meyssignac, B., Ablain, M., 2017. New estimates of the current rate of sea level rise from a sea level budget approach. Geophys. Res. Lett. 44 (8), 3744–3751.
Du, J.L., Yang, S.L., Feng, H., 2016. Recent human impacts on the morphological evolution of the Yangtze River delta foreland: a review and new perspectives. Estuar. Coast. Shelf Sci. 181, 160–169.
Grabemann, I., Uncles, R.J., Krause, G., Stephens, J.A., 1997. Behaviour of turbidity maxima in the Tamar (U.K.) and Weser (F.R.G.) estuaries. Estuar. Coast. Shelf Sci. 45 (2), 235–246.
Guo, L., Xie, W., Xu, F., Wang, X., Zhu, C., Meng, Y., Zhang, W., He, Q., 2021. A historical review of sediment export-import shift in the North branch of Changjiang estuary. Earth Surf. Process. Landf. https://doi.org/10.1002/esp.5084.
He, Y.F., Cheng, H.Q., Chen, J.Y., 2013. Morphological evolution of mouth bars on the Yangtze estuarine waterways in the last 100 years. J. Geogr. Sci. 23, 219–230.
IPCC, Masson-Delmotte, V., Zhai, P., Pirani, A., Connors, S.L., Pean, C., Chen, Y., Goldfarb, L., Gomis, M.I., Mattews, J.B.R., Berger, S., Huang, M., Yelekci, O., Yu, R., Zhou, B., Lonny, E., Maycock, T.K., Waterfield, T., Leitzell, K., Caud, N., 2021. The Physical Basis: Working Group I Contribution to the Sixth Assessment Report of the Inter-government Panel on Climate Change.
Jevrejeva, S., Jackson, L.P., Riva, R.E., Grinsted, A., Moore, J.C., 2016. Coastal sea level rise with warming above 2 °C. Proc. Natl. Acad. Sci. USA 113 (47), 13342.
Jiang, X., Lu, B., He, Y., 2013a. Response of the turbidity maximum zone to fluctuations in sediment discharge from river to estuary in the Changjiang estuary (China). Estuar. Coast. Shelf Sci. 131, 24–30.
Jiang, C.J., de Swart, H.E., Li, J.F., 2013b. Mechanisms of along-channel sediment transport in the North passage of the Yangtze Estuary and their response to large-scale interventions. Ocean Dyn. 63 (2–3), 283–305.
Jiang, C.J., Li, J.F., de Swart, H.E., 2012. Effects of navigational works on morphological changes in the bar area of the Yangtze Estuary. Geomorphology 139, 205–219.
Li, W.H., Cheng, H.Q., Li, J.F., Dong, P., 2008. Temporal and spatial changes of dunes in the Changjiang (Yangtze) estuary, China. Estuar. Coast. Shelf Sci. 77 (1), 169–174.
Liu, B., de Swart, H.E., Jonge, V.N.D., 2018. Phytoplankton bloom dynamics in turbid, well-mixed estuaries: a model study. Estuar. Coast. Shelf Sci. 211, 137–151.

Luan, H.L., Ding, P.X., Wang, Z.B., Ge, J.Z., Yang, S.L., 2016. Decadal morphological evolution of the Yangtze Estuary in response to river input changes and estuarine engineering projects. Geomorphology 265, 12–23.

Mei, X.F., Dai, Z.J., Wei, W., Li, W.H., Wang, J., Sheng, H., 2018. Secular bathymetric variations of the North channel in the Changjiang (Yangtze) estuary, China, 1880–2013: causes and effects. Geomorphology 303, 30–40.

Mitchell, S.B., 2013. Turbidity maxima in four macrotidal estuaries. Ocean Coast. Manag. 79, 62–69.

Pan, L., Ding, P., Ge, J., 2012. Impacts of deep waterway project on morphological changes within the North passage of the Changjiang estuary, China. J. Coast. Res. 28 (5), 1165–1176.

Raymond, J., Martin, G., Broadbent, John, 2004. Chart datum for hydrography. Hydrogr. J. 4 (112), 9–14.

Savenijie, H.H.G., 2012. Salinity and Tides in Alluvial Estuaries (version 2.3). Utrecht: Delft University of Technology, The Netherlands.

Schubel, J.R., 1968. Turbidity maximum of the northern Chesapeake Bay. Science 161, 1013–1015.

Shi, S., Cheng, H.Q., Xuan, X., Hu, F.X., Yuan, X.T., Jiang, Y.H., Zhou, Q.P., 2018. Fluctuations in the tidal limit of the Yangtze River estuary in the last decade. Sci. China Earth Sci. 61 (8), 1–12.

Teng, L.Z., Cheng, H.Q., de Swart, H.E., Dong, P., Li, Z.H., Li, J.F., Wang, Y.J., 2021. On the mechanism behind the shift of the turbidity maximum zone in response to reclamations in the Yangtze (Changjiang) estuary, China. Mar. Geol. 440. https://doi.org/10.1016/j.margeo.2021.106569.

Tessler, Z.D., Vörösmarty, C., Grossberg, M., Gladkova, I., Aizenman, H., Syvitski, J.P.M., Foufoula-Georgiou, E., 2015. Profiling risk and sustainability in coastal deltas of the world. Science 349 (6248), 638–643.

van Maren, D.S., Oost, A.P., Wang, Z., Vos, P.C., 2016. The effect of land reclamations and sediment extraction on the suspended sediment concentration in the Ems estuary. Mar. Geol. 376, 147–157.

Wang, Y.J., Jiang, C.J., Cheng, H.Q., Li, W.H., Teng, L.Z., 2022. Characteristics and driving mechanisms of mixing and stratification in the North passage of the Changjiang estuary, China. J. Coast. Res. 38 (1). https://doi.org/10.2112/JCOASTRES-D-21-00053.1.

Wang, Z.B., Vandenbruwaene, W., Taal, M., Winterwerp, H., 2019. Amplification and deformation of tidal wave in the upper Scheldt estuary. Ocean Dyn. 69 (7), 829–839.

Wei, W., Dai, Z.J., Mei, X.F., Liu, J.P., Gao, S., Li, S.S., 2017. Shoal morphodynamics of the Changjiang (Yangtze) estuary: influences from river damming, estuarine hydraulic engineering and reclamation project. Mar. Geol. 386, 32–43.

Winterwerp, J.C., Wang, Z.B., van Braeckel, A., van Holland, G., Kösters, F., 2013. Man-induced regime shifts in small estuaries-ii: a comparison of rivers. Ocean Dyn. 63, 1293–1306.

Wu, J., Wang, Y., Cheng, H.Q., 2009. Bedforms and bed material transport pathways in the Changjiang (Yangtze) estuary. Geomorphology 104 (3), 175–184.

Wu, S.H., Cheng, H.Q., Xu, Y., Li, J.F., Zheng, S.W., 2016a. Decadal changes in bathymetry of the Yangtze River estuary: human impacts and potential saltwater intrusion. Estuar. Coast. Shelf Sci. 182, 158–169.

Wu, S.H., Cheng, H.Q., Xu, Y., 2016b. Riverbed micromorphology of the Yangtze River estuary. Water 8 (5), 190–204.

Yang, H.F., Yang, S.L., Xu, K.H., Milliman, J.D., Wang, H., Yang, Z., Chen, Z., Zhong, C.Y., 2018. Human impacts on sediment in the Yangtze River: a review and new perspectives. Glob. Planet. Change 162, 8–17.

Yang, S.L., Milliman, J.D., Xu, K.H., Deng, B., Zhang, X.Y., Luo, X.X., 2014. Downstream sedimentary and geomorphic impacts of the Three Gorges Dam on the Yangtze River. Earth-Sci. Rev. 138, 469–486.

Zhang, X., Li, J.F., Zhu, W., Cheng, H.Q., Chen, W., 2015. The self-regulation process and its mechanism of channels' bed changes in the Changjiang (Yangtze) estuary in China. Acta Oceanol. Sin. 34 (7), 123–130.

Zhang, X., Fagherazzi, S., Leonardi, N., Li, J.F., 2018. A positive feedback between sediment deposition and tidal prism may affect the morphodynamic evolution of tidal deltas. J. Geophys. Res., Earth 123 (11), 2767–2783.

Zheng, S.W., Cheng, H.Q., Wu, S.H., Liu, G.W., Lu, X.J., Xu, W.X., 2016a. Discovery and implications of catenary-bead subaqueous dunes. Sci. China Earth Sci. 3, 1–9.

Zheng, S.W., Cheng, H.Q., Zhou, Q., Wu, S.H., Shi, S., Xu, W., 2016b. Morphology and mechanism of the very large dunes in the tidal reach of the Yangtze River, China. Cont. Shelf Res. 139, 54–61.

Zheng, S.W., Xu, Y., Cheng, H.Q., 2018. Riverbed erosion of the final 565 kilometers of the Yangtze River (Changjiang) following construction of the Three Gorges Dam. Sci. Rep. 8 (1), 1–11.

Zheng, S.W., Cheng, H.Q., Lv, J., Li, Z., Zhou, L., 2021. Morphological evolution of estuarine channels influenced by multiple anthropogenic stresses: a case study of the North channel, Yangtze Estuary, China. Estuar. Coast. Shelf Sci. 249. https://doi.org/10.1016/j.ecss.2020.107075.